

PAPER • OPEN ACCESS

Existence of a flat band in highly correlated metal BaCo_2P_2

To cite this article: A Van Der Spuy *et al* 2025 *J. Phys.: Condens. Matter* **37** 155602

View the [article online](#) for updates and enhancements.

You may also like

- [Extended Haldane model- a modern gateway to topological insulators](#)
Tanay Nag and Saptarshi Mandal
- [Spin-orbit torque in a three-fold-symmetric bilayer and its effect on magnetization dynamics](#)
Wuzhang Fang, Edward Schwartz, Alexey A Kovalev *et al.*
- [Dynamical screening in correlated electron systems— from lattice models to realistic materials](#)
Philipp Werner and Michele Casula

Existence of a flat band in highly correlated metal BaCo_2P_2

A Van Der Spuy¹ , R Warmbier²  and Abhishek Pandey^{1,3,*} 

¹ Materials Physics Research Institute, School of Physics, University of the Witwatersrand, Johannesburg 2000, Gauteng, South Africa

² Mandelstam Institute for Theoretical Physics, School of Physics, University of the Witwatersrand, Johannesburg 2000, Gauteng, South Africa

³ Ames Laboratory, Iowa State University, Ames, IA 50011, United States of America

E-mail: abhishek.pandey@wits.ac.za and robert.warmbier@wits.ac.za

Received 30 October 2024, revised 29 January 2025

Accepted for publication 14 February 2025

Published 5 March 2025



CrossMark

Abstract

We report on the observation of a flat band situated at the Fermi level E_F along with the structural, electrical transport, and magnetic properties of BaCo_2P_2 that crystallizes in the ThCr_2Si_2 -type body-center tetragonal structure. This compound has the largest inter-layer pnictide (Pn) distance d_{Pn-Pn} as well as the largest c/a ratio among all the known $A\text{Co}_2Pn_2$ (A = alkaline earth metal) compounds, where a and c are the tetragonal lattice parameters. Hence, the magnetic and electronic properties of this compound are expected to have a quasi-two-dimensional character. Despite the evidence of the presence of sizable magnetic interactions, magnetic susceptibility $\chi(T)$ of BaCo_2P_2 does not show magnetic ordering down to 1.8 K. The material shows good metallic conduction with a large residual resistivity ratio $\rho_{300\text{K}}/\rho_{1.8\text{K}} \approx 70$ and a Fermi liquid behavior at low temperature. Kadowaki–Woods ratio R_{KW} of BaCo_2P_2 suggests the presence of sizable electronic correlations within this system. Additionally, a large many-body enhancement of 2.3 of the experimental density of states $D^\gamma(E_F)$ over the band-structure $D^{\text{band}}(E_F)$ is inferred to arise from sizable electron-electron and/or electron-phonon interactions leading to a substantial deviation from the free-electron behavior.

Supplementary material for this article is available [online](#)

Keywords: strongly-correlated electronic state, flat bands, quasi 2D-structure

1. Introduction

Compounds that crystallize in the layered tetragonal ThCr_2Si_2 structure have attracted significant interest in recent years because of the wide range of exciting physical properties they

exhibit. This includes prototypical heavy Fermion behavior in CeCu_2Si_2 [1] as well as high- T_c unconventional superconductivity in doped BaFe_2As_2 [2]. Both of these observations show that strongly correlated electronic states can lead to exciting ground states in these materials. The general empirical formula for these compounds is AT_2X_2 (A : rare-earth, alkali or alkaline-earth metal, T : transition metal, X : metalloid or pnictide Pn) where the A , T , and X atoms occupy the $2a$, $4d$, and $4e$ Wyckoff sites, respectively [3]. The structure consists of alternating layers of A and $[TX]_2$ ions along the crystallographic c -axis. The $[TX]_2$ layers contain square lattices of T atoms tetrahedrally coordinated by X atoms. The cationic A layers act as electron donors to the adjacent quasi 2-dimensional $[TX]_2$ layers. Based

* Author to whom any correspondence should be addressed.



Original Content from this work may be used under the terms of the [Creative Commons Attribution 4.0 licence](#). Any further distribution of this work must maintain attribution to the author(s) and the title of the work, journal citation and DOI.

on the ratio c/a of the tetragonal lattice parameters, these materials are usually classified as collapsed tetragonal (cT) with X - X inter-layer distance approaching X - X single-bond length and the uncollapsed tetragonal (ucT) with larger X - X inter-layer distances. The structural differences between these two variants have been explained by the presence or lack of X - X interlayer bonding in cT and ucT structures respectively [4]. The magnetic properties of these compounds decisively depend upon the interlayer bonding between the X ions or its absence as this affects the ionic state of the transition metal ion which consequently regulates the spin state. As a result, depending on the type of A ion present in the lattice, the ACo_2Pn_2 compounds adopt ucT or cT structures at ambient pressure and exhibit a variety of magnetic ground states.

Interest in ACo_2Pn_2 materials was instigated after the fascinating discovery of stripe-type antiferromagnetic (AFM) fluctuations in $SrCo_2As_2$ [5] that are believed to be responsible for the realization of Cooper pairs in iron-based superconductors. Later, these Co-based 122 systems led to a plethora of intriguing ground states and tunable structure-property relations. One such example is the observation of a putative quantum critical point (QCP) at $x \sim 0.5$ in $Sr_{1-x}Ca_xCo_2P_2$ as the system transitions from ucT structure to cT structure with increasing x [6]. Similarly, a QCP induced by Ge–Ge dimer-breaking is observed in $SrCo_2(Ge_{1-x}P_x)_2$ at $x \sim 0.33$ as the cT structure of $SrCo_2Ge_2$ transitions to the ucT $SrCo_2P_2$ [7]. Furthermore, some $ThCr_2Si_2$ phosphides such as $BaNi_2P_2$, $LaRh_2P_2$ and $LaRu_2P_2$ have been shown to exhibit a superconducting phase at low temperatures [8, 9]. These exiting observations imply the significance of further investigations focused on the structure-property relationships in unexplored Co-based 122 compounds. In this study, we explore the electronic and physical properties of $BaCo_2P_2$ that has the largest c/a ratio as well as d_{Pn-Pn} distance among the ACo_2Pn_2 compounds. A flat band spanning a significant fraction of the Brillouin zone is present at the Fermi level E_F in this compound and the physical properties suggest highly-correlated electronic states.

2. Experimental and computational details

Density functional theory (DFT) calculations were performed using the GPAW software [10–13] and the r^2 SCAN meta-GGA exchange-correlation functional [14, 15] as implemented in libxc [16]. r^2 SCAN is an all-purpose meta-GGA functional which often leads to better consistency than GGAs for correlated materials. Results obtained with the PBEsol exchange-correlation functional [17, 18] are used as comparison. The influence of DFT + U Hubbard corrections is discussed later and in the supplemental material. Plane-wave energy cutoffs and k -point sampling were chosen as 900 eV and $16 \times 16 \times 6$ Monkhorst–Pack mesh. For the density of states (DOS) calculations, a denser sampling of $50 \times 50 \times 16$ was used. A Fermi–Dirac smearing of 20 meV was used in the self-consistent calculation. The DOS as a function of energy was computed with a spacing of 10 meV per bin. Tetrahedron

integration, as implemented in GPAW, was used here instead of Gaussian smearing as it allows for a higher resolution. Experimentally-derived atomic positions and lattice parameters were used as inputs.

Polycrystalline $BaCo_2P_2$ was synthesized by solid state reaction of high-purity starting elements Ba (99.99%) from Sigma-Aldrich and Co (99.998%) and P (99.999%) from Alfa-Aesar. The pressed pellet was placed in an alumina crucible and sealed in a quartz tube under partial Ar pressure. The assembly was heated to 395 °C in 15 h and held there for 40 h, then heated to 715 °C in 20 h and held there for 40 h, and then heated to 750 °C in 3 h and held there for another 40 h before furnace cooling. The sample was then thoroughly ground, repelletized, and resealed in a quartz tube under partial Ar pressure. The assembly was then heated to 850 °C in 10 h, held there for 30 h, and then heated to 1000 °C in 4 h and held there for 65 h, and then furnace cooled. Room temperature powder x-ray diffraction (XRD) measurement was performed using a Rigaku Geigerflex powder diffractometer equipped with a $Cu-K_{\alpha}$ radiation source. Rietveld refinement was performed using the FullPROF package [19]. Temperature T dependence of electrical resistivity ρ was measured using a physical properties measurement system (PPMS) of quantum design Inc. (QDI), USA [20]. Temperature dependence of magnetic susceptibility as well as isothermal magnetization M versus applied field H were measured using a SQUID-magnetic properties measurement system (MPMS) of QDI.

3. Results and discussion

3.1. Crystal structure

The Rietveld refinement confirms that $BaCo_2P_2$ crystallizes in the $ThCr_2Si_2$ -type tetragonal structure (figure 1). A few small impurity peaks appearing between 28° and 68° could not be indexed to any known phase(s) formed by the constituent elements [21]. The tetragonal lattice parameters a , c , the c -axis P position parameter z_P as well as the distance between the two nearest interlayer P atoms d_{P-P} are listed in table 1 together with the corresponding parameters of the other ACo_2Pn_2 compounds. The c/a ratio of 3.2612(4) and d_{P-P} of 3.811(8) Å of $BaCo_2P_2$ is largest among the ACo_2Pn_2 compounds implying nearly non interacting P layers and hence ensuring a 2+ oxidation state of Co ions. Additionally, the large interlayer distance between the adjacent square lattices of the Co-ions implies a weak magnetic coupling J_c along the crystallographic c direction. Hence, the effective magnetic interactions in $BaCo_2P_2$ are likely quasi two-dimensional.

3.2. Electronic structure

DFT relies on periodic simulation cells implying long-range order. Hence, it can simulate different ordered magnetic configurations but cannot capture the effects of fluctuations in the spin density. Usually, a diamagnetic (DM) configuration is used to obtain the DOS at the E_F and an AFM and/or ferromagnetic (FM) configuration is used to estimate effective

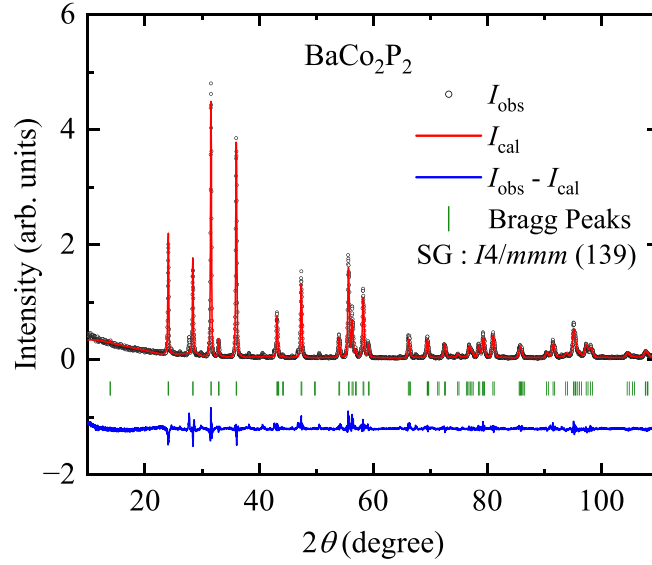


Figure 1. Room temperature powder x-ray diffraction data of BaCo_2P_2 , together with Rietveld refinement profile, difference profile and Bragg positions.

Table 1. Structural parameters of ACo_2Pn_2 ($A = \text{Ca, Sr, Ba}$ and $\text{Pn} = \text{P, As}$). All compounds crystallize in the tetragonal ThCr_2Si_2 structure with space group $I4/mmm$ (SG: 139). The listed crystallographic parameters are the unit cell parameters a , c , c/a , the z position of the Pn atoms z_{Pn} , and the distance between two nearest inter-layer Pn atoms $d_{\text{Pn}-\text{Pn}}$.

Structure parameter	CaCo_2P_2 [22]	SrCo_2P_2 [22]	BaCo_2P_2 (This work)	CaCo_2As_2 [23, 24]	SrCo_2As_2 [25]	BaCo_2As_2 [26]
Structure variant	cT	T	T	cT	T	T
a (Å)	3.858(1)	3.794(1)	3.8059(2)	3.989(3)	3.9471(4)	3.95743(2)
c (Å)	9.593(1)	11.610(1)	12.4119(5)	10.33(1)	11.801(1)	12.66956(9)
c/a	2.487	3.060	3.2612(4)	2.59	2.9898(6)	3.20146(4)
z_{Pn}	0.3721(4)	0.3525(5)	0.3465(3)	0.372	0.3588(1)	0.35087(3)
$d_{\text{Pn}-\text{Pn}}$ (Å)	2.454(6)	3.424(8)	3.811(8)	2.64	3.333(3)	3.7728(8)

magnetic moments and upper bounds for the spin–spin interaction. For both PBEsol and $r^2\text{SCAN}$ functionals G- or Néel-type AFM configuration is suppressed for BaCo_2P_2 converging to DM solutions [27, 28]. For a comparative analysis, we also performed calculations for magnetic ordered configurations as described in the following. The A-type AFM configuration, which exhibits intra-layer FM coupling, produces the magnetic moment of $\mu = 0.36$ and $0.59 \mu_B$, respectively, for PBEsol and $r^2\text{SCAN}$. These values are small compared to $1.47 \mu_B$ estimated from the experiment (table 2). Further, the experimental results discussed below suggest the presence of correlated electronic states. We, therefore, included DFT + U Hubbard corrections and found that the A-type AFM magnetic moment is only weakly influenced by the Hubbard parameter. However, $U_{\text{PBE}} = 3.1 \text{ eV}$ and $U_{r^2\text{SCAN}} = 1.15 \text{ eV}$ were adequate to yield $\mu \approx 1.5 \mu_B$ per Co atom for the Néel-type AFM configuration (figure 2). At these values for the Hubbard correction the $E_{\text{AFM}} - E_{\text{DM}}$ is -0.20 eV for $r^2\text{SCAN}$, and -0.25 eV for PBEsol.

ThCr_2Si_2 -type ucT materials are layered and often exhibit quasi-two-dimensional characteristics in electronic as well magnetic properties. As a consequence, the electronic structure often exhibits bands with little or no dispersion,

commonly referred to as flat bands [25, 29]. In BaCo_2P_2 , flat bands close to the E_F can be found along the $\text{M}-\Gamma$, $\Gamma-\text{Z}$, and $\text{A}-\text{Z}$ directions (figure 2). One of the two flat bands along $\text{M}-\Gamma$ is close to the E_F , but its exact position depends on the details of the computation. With the parameters used here, the bands sit at E_F in $r^2\text{SCAN}$, below E_F in PBEsol, and above E_F if Hubbard corrections are applied to either functional. The latter might be an artifact of the Hubbard correction. To put these results into context we compare the band structure of the non-magnetic configuration of BaCo_2P_2 to those of BaCo_2As_2 and SrCo_2P_2 computed with $r^2\text{SCAN}$ without Hubbard correction (figure 3), as it is not possible to ascertain equivalent values of Hubbard U consistently. The E_F is lower for BaCo_2As_2 so that the flat band at E_F is along the $\Gamma-\text{Z}$ rather than the $\text{M}-\Gamma$ direction. This is a significant difference as the $\Gamma-\text{Z}$ path is perpendicular to the basal ab -plane while the $\text{M}-\Gamma$ is within the basal plane. Additionally, only the flat band along the $\Gamma-\text{Z}$ is completely dispersion free. In the case of SrCo_2P_2 the two flat bands along $\text{M}-\Gamma$ path are only 10 meV apart, hence, they appear to merge. The flat bands along $\text{M}-\Gamma$ as well as $\text{A}-\text{Z}$ paths are both close to the E_F and both are parallel to the basal plane. Accordingly, one can expect SrCo_2P_2 to have the largest and BaCo_2As_2 to have the smallest DOS at the E_F .

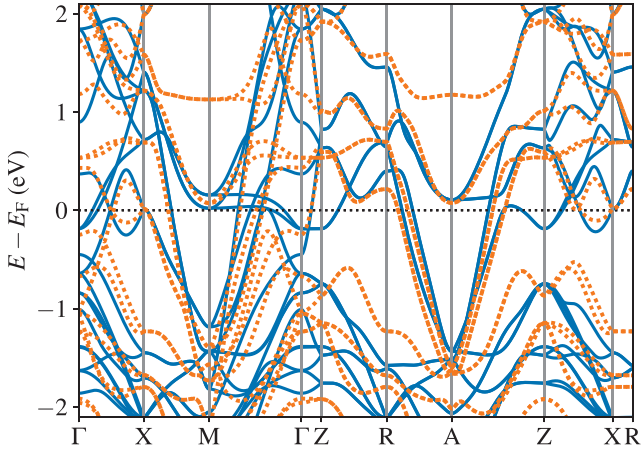


Figure 2. Band structure of BaCo_2P_2 computed with $r^2\text{SCAN} + U$ (1.15 eV) is presented. The blue solid lines refer to the nonmagnetic/diamagnetic configuration, the orange dashed line refers to the Néel-type AFM configuration.

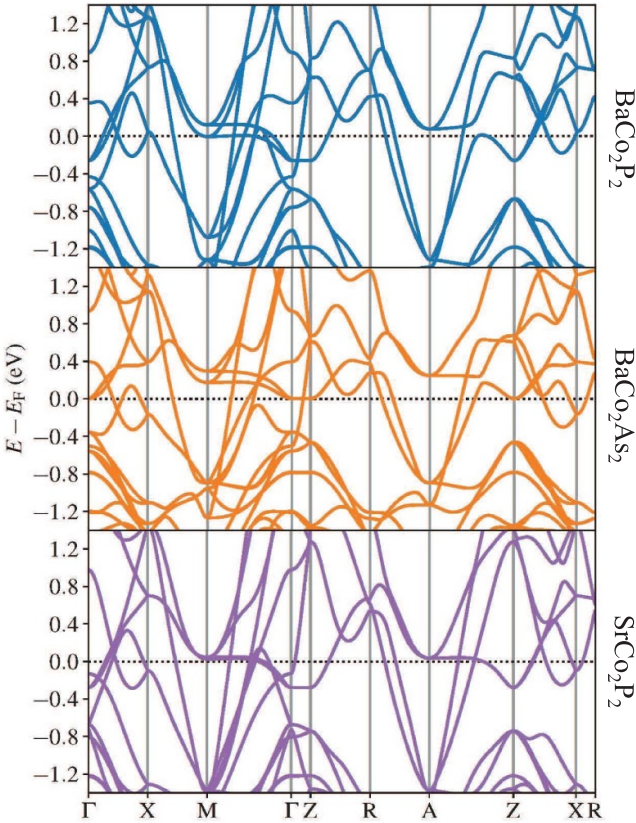


Figure 3. Band structure of nonmagnetic configuration of BaCo_2P_2 (upper panel), BaCo_2As_2 (middle panel), and SrCo_2P_2 (lower panel) computed with $r^2\text{SCAN}$ without Hubbard corrections.

The total and projected DOS of the nonmagnetic configuration of BaCo_2P_2 are shown in figures 4(a) and (c), respectively. The DOS around the E_F is dominated by the Co d_{xy} -orbital, which points to neighboring Co atoms. The maximum DOS near the E_F is $D^{\text{band}}(E_F) = 6.68$ states (eV f.u.) $^{-1}$. While the exact position of this maximum with respect to the E_F depends

delicately on the xc-functional and the Hubbard correction, the height is relatively stable. Without Hubbard corrections we get $D^{\text{band}}(E_F) = 6.86$ states (eV f.u.) $^{-1}$ with $r^2\text{SCAN}$ and $D^{\text{band}}(E_F) = 7.09$ states (eV f.u.) $^{-1}$ with PBEsol. Considering these variations, we estimate the DOS at E_F as $D^{\text{band}}(E_F) = 6.9(2)$ states (eV f.u.) $^{-1}$. In the Néel-type AFM configuration the d_{xy} -orbital is pushed up by about 1.1 eV away from the E_F (figures 4(b) and (d)). The d_{xy} -orbital peak at 0.5 eV is not present in the nonmagnetic configuration. Notably the valence band region of the AFM DOS is very different from the nonmagnetic case. While this magnetically ordered configuration is of lowest energy, it likely does not describe the real system, especially since it needed the extra Hubbard corrections to emerge. Further, as discussed below, no evidence of any type of magnetic ordering has been experimentally observed.

The Fermi surface of the nonmagnetic configuration of BaCo_2P_2 obtained using PBEsol and plotted using FermiSurfer [30] is nested with five distinct contributions (figure 5). The dark blue cones in the corners stem from the flat band along the M - Γ path. The color coding refers to the Fermi velocity v_F , which is very small, about 0.01 Rydberg atomic units (RAU) for the flat bands, where $1 \text{ RAU} \approx 1.094 \times 10^6 \text{ m s}^{-1}$. The largest v_F is found closer to the center of the Brillouin zone in several places stemming from the steep bands crossing the E_F , such as between Γ and Z, X and M, and R and A (figure 2). With a value of 0.71 RAU, the v_F of BaCo_2P_2 is close to ~ 1 RAU found in simple metals.

3.3. Electrical transport

Electrical resistivity ρ versus temperature T of the polycrystalline BaCo_2P_2 shows metallic T -dependence with a large residual resistivity ratio (RRR) $\rho_{300\text{K}}/\rho_{1.8\text{K}}$ of 69.5 and a slight negative curvature for $T \gtrsim 150$ K (figure 6). Similar negative curvatures were also seen in CaCo_2P_2 [31], SrCo_2P_2 [32–34], and BaCo_2As_2 [26, 35]. Consistent with the heat capacity $C_p(T)$ measurements [36], no phase transition is evident down to 1.8 K. A negative curvature is often seen in metals that have sizable presence of d bands near the E_F , as this can lead to substantial sd interband scattering [37] contributing a $-DT^3$ term to the $\rho(T)$. Hence, to account for the negative curvature, an additional $-DT^3$ term was added to the Bloch–Grüneisen (BG) model [38]. We fitted the $\rho(T)$ data using

$$\rho(T) = \rho_0 + \rho_{\text{BG}}(T) - DT^3, \quad (1)$$

where the residual resistivity ρ_0 was held fixed at the experimental value of $2.79 \mu\Omega \text{ cm}$. The $\rho_{\text{BG}}(T)$ was approximated using a high accuracy Padé approximant [39]. A satisfactory fit was obtained with the fit parameters $\Theta_R = 260(2)$ K, $\rho(\Theta_R) = 184(2) \mu\Omega \text{ cm}$, and $D = 6.2(3) \times 10^{-7} \mu\Omega \text{ cm K}^{-3}$. The $\rho(T)$ of BaCo_2P_2 exhibits a T^2 -dependence for $T \lesssim 45$ K suggesting a Fermi liquid behavior at low temperatures (Inset, figure 6). Hence, the $\rho(T)$ data below 45 K were fitted using $\rho(T) = \rho_0 + AT^2$, yielding $A = 4.4(4) \times 10^{-3} \mu\Omega \text{ cm K}^{-2}$. The parameters obtained from the $\rho(T)$ data fits are listed in table 2.

The Kadowaki–Woods ratio $R_{\text{KW}} = A/\gamma^2$ is an empirically determined parameter that is often used to evaluate the strength

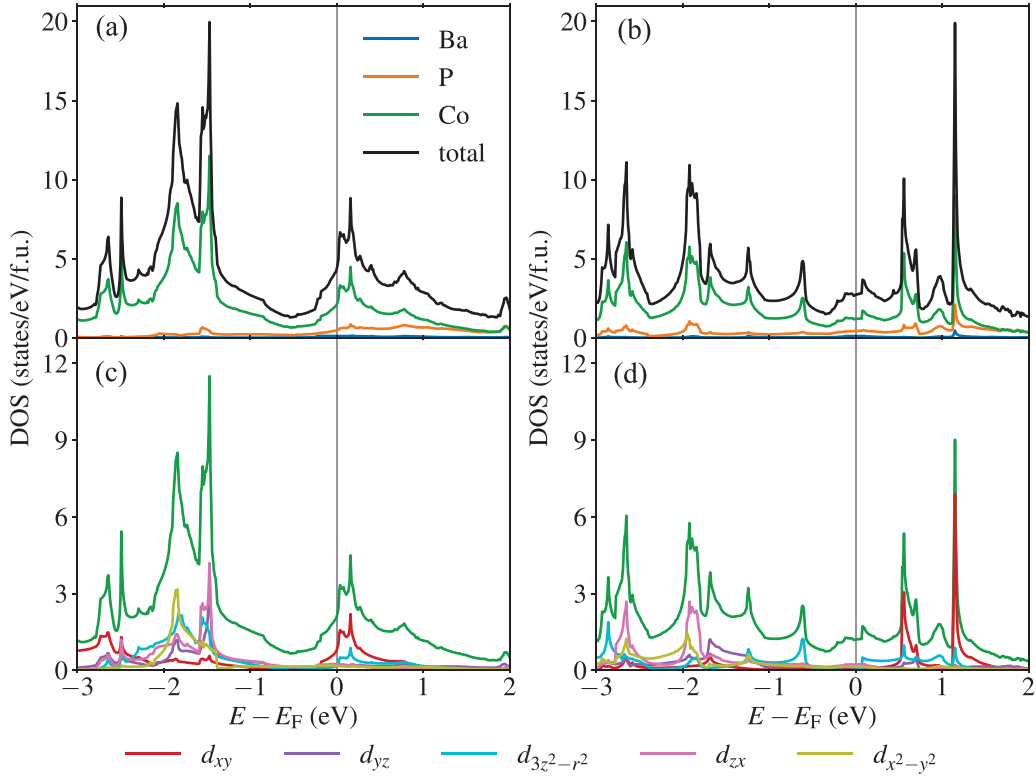


Figure 4. Total and atom-decomposed density of states (DOS) of BaCo_2P_2 computed with $r^2\text{SCAN} + \text{U}(1.15 \text{ eV})$ for (a) nonmagnetic/diamagnetic and (b) Néel-type AFM configuration. Partial DOS of the Co d -orbitals are shown in (c) and (d) for nonmagnetic/diamagnetic and (b) Néel-type AFM configuration, respectively.

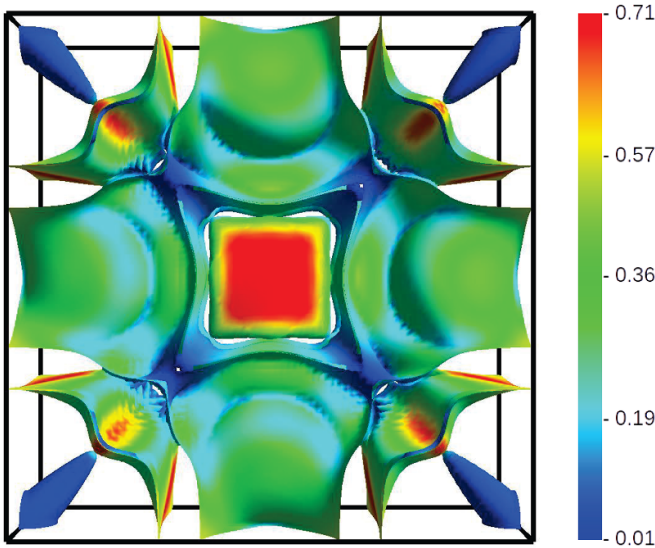


Figure 5. A 3D rendering of the Fermi-surface as viewed from the top is shown. The color coding represents the Fermi velocity ranging from 0.01 atomic units (blue) to 0.71 atomic units (red).

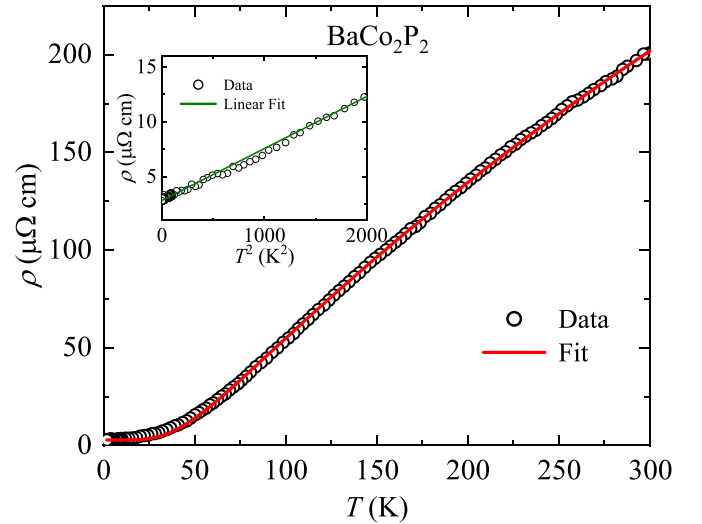


Figure 6. Temperature T dependence of electrical resistivity ρ of BaCo_2P_2 . Solid red curve is a fit by the Bloch–Grüneisen model with an additional $-DT^3$ term due to Mott sd -scattering as described in the text. Inset: ρ plotted as a function of T^2 for $T \leq 44 \text{ K}$. Solid green line is a linear fit to the data.

of electronic correlations within metallic systems [40, 41]. It has been found that materials within the same class typically have similar values of R_{KW} . Figure 7 shows the R_{KW} ratio of BaCo_2P_2 along with the other ACo_2P_2 compounds as well as BaCo_2As_2 in relation to the values obtained for heavy fermions [40] and transition metals [42]. The R_{KW} of

BaCo_2P_2 and the other ACo_2P_2 lie below the nearly linear trend observed in heavy fermion systems but above that of transition metals suggesting a high degree of electronic correlations present in 122 phosphides.

Table 2. Physical properties parameters of ACo_2P_2 ($A = Ca, Sr, Ba$) and $BaCo_2As_2$. The listed parameters are those obtained from heat capacity $C_p(T)$ measurements namely Sommerfeld coefficient γ , density of states at Fermi energy $D^\gamma(E_F)$, coefficient β of lattice heat capacity, Debye temperature Θ_D obtained at low T as well as all T , Einstein temperature Θ_E , fractional contribution m of the Einstein term. It must be clarified that the Θ_D (All T) of $BaCo_2P_2$ has been determined using the Debye–Einstein model, while that for $BaCo_2As_2$ [26] is estimated using the Debye model only. The parameters obtained from electrical resistivity $\rho(T)$ measurements are residual resistivity ρ_0 at $T = 1.8$ K, residual resistivity ratio (RRR), Debye temperature Θ_R , coefficient A of T^2 term, and coefficient D of Mott sd scattering term. The other reported parameters are the density of states $D^{\text{bands}}(E_F)$ obtained from band structure calculations, Kadowaki–Woods ratio R_{KW} , effective paramagnetic moment μ_{eff} , and paramagnetic Weiss temperature θ_p .

Parameter	CaCo ₂ P ₂ [31]	SrCo ₂ P ₂ [32–34]	BaCo ₂ P ₂ (This work, [36])	BaCo ₂ As ₂ [26, 35]
γ (mJ/mol K ²)	23	39.6	36.9(6)	44.39(3)
$D^\gamma(E_F)$ (states/eV f.u.)	9.8	16.8	15.6(3)	18.82(2)
$D^{\text{band}}(E_F)$ (states/eV f.u.)	7.3	6.9	6.9(2)	8.5
$D^\gamma(E_F)/D^{\text{band}}(E_F)$	1.34	2.5	2.3(2)	~ 2
β (mJ/mol K ⁴)	0.107	—	0.22(3)	0.319(3)
Θ_D (K) (Low T)	≈ 450	—	354(17)	312(2)
Θ_D (K) (All T)	—	—	616(10)	301(3)
Θ_E (K) (All T)	—	—	148(3)	—
m	—	—	0.42(2)	—
ρ_0 ($\mu\Omega$ cm)	—	0.42	2.79	5.10(2)
$\rho(\Theta_R)$ ($\mu\Omega$ cm)	—	—	184(2)	61(2)
RRR	~ 5	75	69.5	21.8
Θ_R (K)	—	—	260(2)	174(5)
A ($10^{-3} \mu\Omega$ cm K ⁻²)	≈ 3.2	0.97	4.4(4)	3.94(1)
D ($10^{-7} \mu\Omega$ cm K ⁻³)	—	—	6.2(3)	—
R_{KW} ($10^{-3} \text{ m}\Omega$ cm mol ² J ⁻² K ²)	≈ 6	~ 0.62	3.2	2.0
μ_{eff} ($\mu_B/\text{Co atom}$)	≈ 1.1 ($\parallel c$ -axis)	1.53 ($\parallel c$ -axis)	1.47(3)	—
	≈ 1.0 ($\perp c$ -axis)	1.59 ($\parallel a$ -axis)	—	—
θ_p (K)	92 K ($\parallel c$ -axis)	-90.0 K ($\parallel c$ -axis)	-102(8)	—
	101 K ($\perp c$ -axis)	-95.2 K ($\parallel a$ -axis)	—	—

3.4. Magnetism

Magnetization M of $BaCo_2P_2$ varies linearly with the applied magnetic field H for $T \geq 50$ K and shows a sublinear variation with a slight negative curvature at $T = 5$ and 10 K (figure 8). We attribute this negative curvature to the presence of trace amounts of saturable paramagnetic impurities. The T -dependence of magnetic susceptibility $\chi = M/H$ does not show evidence of any type of long-range magnetic ordering (figure 9). To determine the intrinsic $\chi(T)$ at low temperatures, corrected for the effects of trace impurities, the gradients of $M(H)$ isotherms at high fields (> 1 T) were obtained by linear fits at $T = 5, 10,$ and 50 K (figure 9). The upturn observed in the $\chi(T)$ at low $T < 10$ K lies above the intrinsic susceptibilities obtained from the high field slopes suggesting that it originates from trace saturable paramagnetic impurities.

The $\chi(T)$ data at high temperatures exhibits paramagnetic behavior and is fitted with the Curie-Weiss law for $200 \text{ K} \leq T < 350 \text{ K}$ using

$$\chi(T) = \frac{C}{T - \theta_p}. \quad (2)$$

The fitted parameters are the Curie constant $C = 0.54(2) \text{ cm}^3 \text{ K/mol}$ and Weiss temperature $\theta_p = -102(8) \text{ K}$. The negative θ_p suggests a sizable presence of AFM interactions. Similar values of θ_p have been reported for a few

other Co-based $122 ACo_2Pn_2$ compounds [25, 34]. Absence of magnetic ordering and large negative θ_p infers a possible presence of AFM fluctuations similar to those obtained in $SrCo_2As_2$ [25]. Using the fitted value of C and assuming $g = 2$, we determine the effective magnetic moment per Co atom $\mu_{\text{eff}} = \sqrt{8C}/\sqrt{2} = 1.47(3) \mu_B$. This value is close to $1.73 \mu_B$ of a $S = 1/2$ ion but is smaller than $3.87 \mu_B$ of high-spin $S = 3/2$ of localized Co^{2+} ions with complete orbital angular momentum quenching. This suggests that even though the $\chi(T)$ exhibits a Curie–Weiss law at high temperatures the magnetic moment of the Co-ions have itinerant character. If we assume a local moment character of Co spins then the Heisenberg model for identical crystallographically equivalent ions can be used to calculate the exchange constants using

$$\theta_p = \frac{-S(S+1)}{3k_B} \sum_j J_{ij}, \quad (3)$$

where the sum runs over all interacting neighbors j for a given spin i [43]. Further, considering the large interlayer distance along the crystallographic c -axis between the Co-sublattice of $BaCo_2P_2$, one can neglect the interlayer interactions J_c . Now, quasi-2D nearest and next-nearest exchange interactions within the Co-square lattice lead to

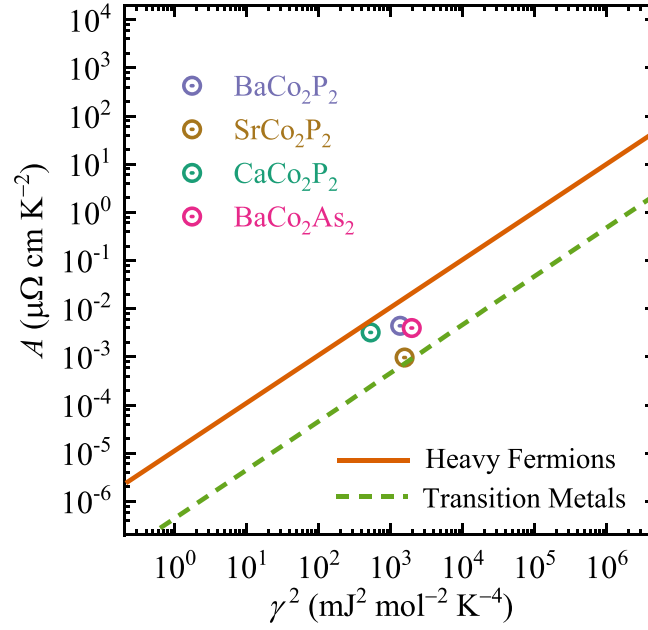


Figure 7. Kadowaki–Woods ratios R_{KW} of ACo_2P_2 ($A = Ca, Sr, Ba$) as well as $BaCo_2As_2$ in comparison to those of heavy fermion systems and transition metals.

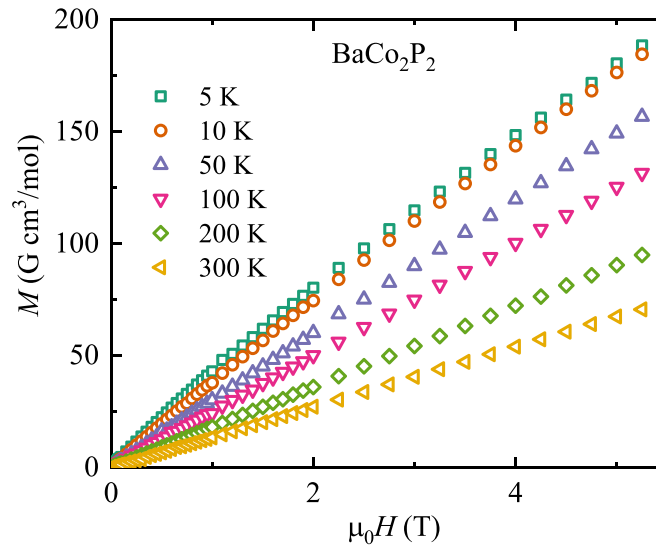


Figure 8. Isothermal magnetization M of $BaCo_2P_2$ as a function of applied magnetic field H measured at the six different temperatures.

$$\theta_p = -\frac{J_1 + J_2}{k_B}. \quad (4)$$

Using $\theta_p = -102(8)$ K, we get the estimate of intra-layer exchange interactions as $J_1 + J_2 = 8.8(7)$ meV, which is equal to that estimated for isostructural $SrCo_2As_2$ within the errors. We further emphasize that applying the Curie–Weiss law to a system of possible itinerant characters may lead to erroneous values of the estimated parameters. However, despite this limitation, the analysis does provide a meaningful insight into the underlying magnetic interactions and the ground state properties of the system.

4. Conclusion

An investigation of the electronic and physical properties of layered tetragonal $BaCo_2P_2$ is reported. This material has the largest interlayer Pn distance as well as the largest c/a ratio, making it the most ‘uncollapsed’ member of the ACo_2Pn_2 family. As a result, magnetic and electronic properties of this system are presumably quasi-two-dimensional. The electronic structure calculations show the presence of a flat-band originating from $Co-d_{xy}$ states close to the E_F along the $M-\Gamma$ direction. The material does not show magnetic ordering down to 1.8 K and observations suggest itinerant behavior of spins with an effective magnetic moment of $1.47(3) \mu_B/Co$ atom. The DFT calculations predict significantly lower local magnetic

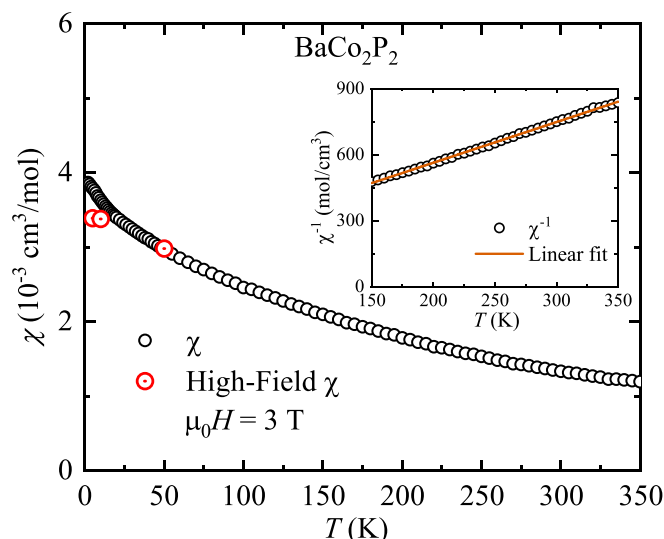


Figure 9. Zero-field-cooled magnetic susceptibility $\chi = M/H$ of polycrystalline BaCo_2P_2 as a function of temperature T measured in an applied magnetic field $\mu_0 H = 3.0$ T. The red circles represent the χ values obtained from fitting the low- T isotherms with linear fits at high fields ($\mu_0 H > 3$ T).

moments than the experimental value, supporting the itinerant nature. Electrical transport measurements exhibit metallic behavior associated with a negative curvature at high temperatures and Fermi liquid behavior at low temperatures. The origin of the negative curvature is attributed to the substantial presence of Co- d states at the E_F leading to interband sd scattering. The estimated Kadowaki-Woods ratio shows a sizable presence of electronic correlations within the material. Despite being polycrystalline, BaCo_2P_2 sample shows a high RRR and a low value of residual resistivity. Considering the anomalous electrical transport properties of related KCo_2As_2 , which also has a high c/a ratio, further investigations focused on the electrical transport properties of a single crystals of BaCo_2P_2 seems important.

Data availability statement

GPAW input and output files are available at the open data repository with the following DOI: <https://doi.org/10.5281/zenodo.14755153>.

All data that support the findings of this study are included within the article (and any supplementary files).

Acknowledgments

R W acknowledges the Centre for High Performance Computing (CHPC), South Africa, for providing computational resources to this research project. This work is based on the research supported in part by the National Research Foundation of South Africa (Ref Numbers: SRUG2205098188). A P acknowledges the financial support from the Friedel Sellschop fellowship of the University of the Witwatersrand, South Africa. We acknowledge Dr B S Jacobs for her suggestions and proofreading this manuscript. The work at Ames Laboratory was supported by

the U.S. Department of Energy, Office of Basic Energy Sciences, Division of Materials Sciences and Engineering. Ames Laboratory is operated for the U.S. Department of Energy by Iowa State University under Contract No. DE-AC02-07CH11358.

Conflict of interest

The authors declare no competing interests.

ORCID iDs

A Van Der Spuy  <https://orcid.org/0009-0000-3816-8931>

R Warmbier  <https://orcid.org/0000-0001-8508-4095>

Abhishek Pandey  <https://orcid.org/0000-0003-2839-1720>

References

- [1] Steglich F, Aarts J, Bredl C D, Lieke W, Meschede D, Franz W and Schäfer H 1979 *Phys. Rev. Lett.* **43** 1892
- [2] Rotter M, Tegel M and Johrendt D 2008 *Phys. Rev. Lett.* **101** 107006
- [3] Shatruk M 2019 *J. Solid State Chem.* **272** 198
- [4] Hoffmann R and Zheng C 1985 *J. Phys. Chem.* **89** 4175
- [5] Jayasekara W et al 2013 *Phys. Rev. Lett.* **111** 157001
- [6] Imai M, Michioka C, Ohta H, Matsuo A, Kindo K, Ueda H and Yoshimura K 2014 *Phys. Rev. B* **90** 014407
- [7] Jia S, Jiramongkolchai P, Suchomel M R, Toby B H, Checkelsky J G, Ong N P and Cava R J 2011 *Nat. Phys.* **7** 207
- [8] Mine T, Yanagi H, Kamiya T, Kamihara Y, Hirano M and Hosono H 2008 *Solid State Commun.* **147** 111
- [9] Jeitschko W, Glaum R and Boonk L 1987 *J. Solid State Chem.* **69** 93
- [10] Mortensen J J et al 2024 *J. Chem. Phys.* **160** 092503
- [11] Larsen A H et al 2017 *J. Phys.: Condens. Matter.* **29** 273002
- [12] Enkovaara J et al 2010 *J. Phys.: Condens. Matter.* **22** 253202

- [13] Mortensen J J, Hansen L B and Jacobsen K W 2005 *Phys. Rev. B* **71** 035109
- [14] Furness J W, Kaplan A D, Ning J, Perdew J P and Sun J 2020 *J. Phys. Chem. Lett.* **11** 8208
- [15] Furness J W, Kaplan A D, Ning J, Perdew J P and Sun J 2020 *J. Phys. Chem. Lett.* **11** 9248
- [16] Lehtola S, Steigemann C, Oliveira M J T and Marques M A L 2018 *SoftwareX* **7** 1
- [17] Perdew J P, Ruzsinszky A, Csonka G I, Vydrov O A, Scuseria G E, Constantin L A, Zhou X and Burke K 2008 *Phys. Rev. Lett.* **100** 136406
- [18] Constantin L A, Perdew J P and Pitarke J M 2009 *Phys. Rev. B* **79** 075126
- [19] Rodríguez-Carvajal J 1993 *Physica B* **192** 55 (see also <https://www.ill.eu/sites/fullprof/>)
- [20] The $\rho(T)$ at $H = 0$ showed a tiny spurious peak close to 30 K. This anomaly disappeared in presence of an applied magnetic field and the observed magnetoresistance was negligible in the entire T -range of our measurement. Hence, the $\rho(T)$ data collected at $H = 8$ T are discussed in the paper.
- [21] The attempts to match these peaks with the reported structures in inorganic crystal structure database, materials project and springer materials databases were not successful.
- [22] Mewis A 1980 *Z. Naturforsch.* **35b** 141
- [23] Pfisterer M and Nagorsen G 1980 *Z. Naturforsch.* **35b** 703
- [24] Pfisterer M and Nagorsen G 1983 *Z. Naturforsch.* **38b** 811
- [25] Pandey A *et al* 2013 *Phys. Rev. B* **88** 014526
- [26] Anand V K *et al* 2014 *Phys. Rev. B* **90** 064517
- [27] The KTBM23 meta-GGA functional [28] was able to produce Néel-type AFM configurations. This functional is however not widely tested yet and is therefore not presented here.
- [28] Kovács P, Tran F, Blaha P and Madsen G K H 2022 *J. Chem. Phys.* **157** 094110
- [29] Li Y *et al* 2019 *Phys. Rev. Lett.* **122** 117204
- [30] Kawamura M 2019 *Comput. Phys. Commun.* **239** 197
- [31] Baumbach R E, Sidorov V A, Lu X, Ghimire N J, Ronning F, Scott B L, Williams D J, Bauer E D and Thompson J D 2014 *Phys. Rev. B* **89** 094408
- [32] Teruya A, Nakamura A, Takeuchi T, Harima H, Uchima K, Hedo M, Nakama T and Ōnuki Y 2014 *J. Phys. Soc. Japan* **83** 113702
- [33] Götze K *et al* 2021 *Phys. Rev. B* **104** 085148
- [34] Imai M, Michioka C, Ueda H, Matsuo A, Kindo K and Yoshimura K 2017 *J. Phys.: Conf. Ser.* **868** 012015
- [35] Sefat A S, Singh D J, Jin R, McGuire M A, Sales B C and Mandrus D 2009 *Phys. Rev. B* **79** 024512
- [36] Sangeetha N S, Cuervo-Reyes E, Pandey A and Johnston D C 2016 *Phys. Rev. B* **94** 014422
- [37] Mott N F 1936 *Proc. R. Soc. A* **153** 699
- [38] Blatt F J 1968 *Physics of Electronic Conduction in Solids* (McGraw-Hill)
- [39] Goetsch R J, Anand V K, Pandey A and Johnston D C 2012 *Phys. Rev. B* **85** 054517
- [40] Kadowaki K and Woods S B 1986 *Solid State Commun.* **58** 507
- [41] Jacko A, Fjærestad J and Powell B 2009 *Nat. Phys.* **5** 422
- [42] Rice M J 1968 *Phys. Rev. Lett.* **20** 1439
- [43] Johnston D C 2012 *Phys. Rev. Lett.* **109** 077201